PLOS | COMPUTATIONAL BIOLOGY

RESEARCH ARTICLE

How to Distinguish Conformational Selection and Induced Fit Based on Chemical Relaxation Rates

Fabian Paul[1,2]*, **Thomas R. Weikl**[1]*

1 Max Planck Institute of Colloids and Interfaces, Department of Theory and Bio-Systems, Potsdam, Germany, **2** Free University Berlin, Department of Mathematics and Computer Science, Berlin, Germany

* fabian.paul@mpikg.mpg.de (FP); thomas.weikl@mpikg.mpg.de (TRW)

OPEN ACCESS

Citation: Paul F, Weikl TR (2016) How to Distinguish Conformational Selection and Induced Fit Based on Chemical Relaxation Rates. PLoS Comput Biol 12(9): e1005067. doi:10.1371/journal.pcbi.1005067

Editor: Nikolay V. Dokholyan, University of North Carolina at Chapel Hill, UNITED STATES

Received: March 18, 2016

Accepted: July 14, 2016

Published: September 16, 2016

Data Availability Statement: All relevant data are within the paper.

Funding: This work was supported by Deusche Forschungsgemeinschaft http://www.dfg.de/en/ collective grant SFB 1114 http://gepris.dfg.de/gepris/projekt/235221301?language=en (to FP TRW). The funders had no role in study design, data collection and analysis, decision to publish, or preparation of the manuscript.

Competing Interests: The authors have declared that no competing interests exist.

Abstract

Protein binding often involves conformational changes. Important questions are whether a conformational change occurs prior to a binding event ('conformational selection') or after a binding event ('induced fit'), and how conformational transition rates can be obtained from experiments. In this article, we present general results for the chemical relaxation rates of conformational-selection and induced-fit binding processes that hold for all concentrations of proteins and ligands and, thus, go beyond the standard pseudo-first-order approximation of large ligand concentration. These results allow to distinguish conformational-selection from induced-fit processes—also in cases in which such a distinction is not possible under pseudo-first-order conditions—and to extract conformational transition rates of proteins from chemical relaxation data.

Author Summary

The function of proteins is affected by their conformational dynamics, i.e. by transitions between lower-energy ground-state conformations and higher-energy excited-state conformations of the proteins. Advanced NMR and single-molecule experiments indicate that higher-energy conformations in the unbound state of proteins can be similar to ground-state conformations in the bound state, and vice versa. These experiments illustrate that the conformational change of a protein during binding may occur before a binding event, rather than being induced by this binding event. However, determining the temporal order of conformational transitions and binding events typically requires additional information from chemical relaxation experiments that probe the relaxation kinetics of a mixture of proteins and ligands into binding equilibrium. These chemical relaxation experiments are usually performed and analysed at ligand concentrations that are much larger than the protein concentrations. At such high ligand concentrations, the temporal order of conformational transitions and binding events can only be inferred in special cases. In this article, we present general equations that describe the dominant chemical relaxation kinetics for all protein and ligand concentrations. Our general equations allow

to clearly infer from relaxation data whether a conformational transition occurs prior to a binding event, or after the binding event.

Introduction

Protein function often involves conformational changes during the binding to ligand molecules [1]. Advanced NMR experiments [2–7] and single-molecule spectroscopy [8–10] indicate that these conformational changes can occur without ligand, or with bound ligand and thus point to an intrinsic conformational dynamics of the proteins. An important question is how the conformational dynamics is coupled to the binding events. Two mechanisms for this coupling are 'conformational selection' [11] and 'induced fit' [12] (see Fig 1(a) and 1(b)). In conformational-selection binding, a conformational change occurs *prior to* the binding of a ligand molecule, as a conformational excitation from the unbound-ground state conformation of the protein. In this mechanism, the ligand seems to 'select' and stabilize a higher-energy conformation for binding. In induced-fit binding, the conformational change occurs *after* ligand binding and is a conformational relaxation into the bound ground-state conformation that is apparently 'induced' by the ligand. These two mechanisms are in particular plausible for small ligand molecules that can quickly 'hop' in and out of the protein binding pocket, i.e. that can enter and exit this binding pocket within transition times that are significantly smaller than the residence or dwell times of the proteins in the different conformations [13].

A central problem is to identify protein binding mechanisms based on experimental data [13–24]. Advanced NMR experiments and single-molecule spectroscopy can reveal higher-energy conformations that are necessary for conformational-selection or induced-fit binding,

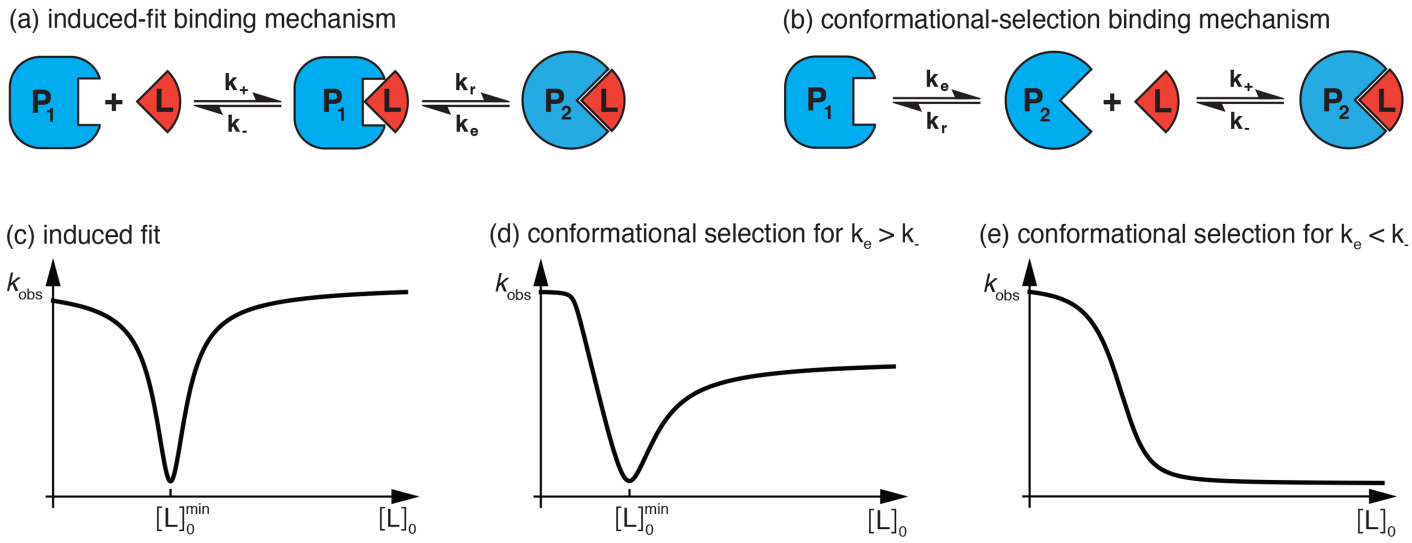

Fig 1. Characteristic chemical relaxation of induced-fit and conformational-selection binding. (a) In induced-fit binding, the change between the conformations P_1 and P_2 of the protein occurs after binding of the ligand L. The intermediate state P_1L relaxes into the bound ground state P_2L with rate k_r, and is excited from the ground state with rate k_e. (b) In conformational-selection binding, the conformational change of the protein occurs prior to ligand binding. The intermediate state P_2 is excited from the unbound ground state P_1 with rate k_e, and relaxes back into the ground state with rate k_r. (c) The dominant, smallest relaxation rate k_{obs} of induced-fit binding is minimal at the total ligand concentration $[L]_0^{min} = [P]_0 - K_d$ where $[P]_0$ is the total protein concentration and K_d the overall dissociation constant. As a function of $[L]_0$, the dominant rate k_{obs} is symmetric with respect to this minimum. (d) The dominant, smallest relaxation rate k_{obs} of conformational-selection binding has a characteristic minimum as a function of $[L]_0$ for $k_e > k_-$, but is not symmetric with respect to this minimum. (e) The dominant rate k_{obs} of conformational-selection binding decreases monotonically with $[L]_0$ for $k_e < k_-$.

doi:10.1371/journal.pcbi.1005067.g001

but do not directly indicate the binding mechanism because such higher-energy conformations may exist both in the bound and unbound state of the protein [4, 8]. In principle, both conformational-selection or induced-fit binding then are possible. Standard mixing or temperature-jump experiments that probe the chemical relaxation into the binding equilibrium can provide additional information that allows to identify the binding mechanism [22, 25–28]. Of particular interest is the dominant, slowest relaxation rate $k_{\rm obs}$ observed in the experiments, and how this rate depends on the total ligand concentration $[{\rm L}]_0$ [22, 25, 28]. The chemical relaxation experiments are often performed and analysed under pseudo-first-oder conditions, i.e. at ligand concentrations that greatly exceed the protein concentrations [22, 25, 29–36]. In the case of induced-fit binding, the dominant relaxation rate $k_{\rm obs}$ *increases* monotonically with the ligand concentration $[{\rm L}]_0$ under pseudo-first-oder conditions. In the case of conformational-selection binding, $k_{\rm obs}$ *decreases* monotonically with increasing $[{\rm L}]_0$ for conformational excitation rates $k_e < k_-$, and *increases* monotonically with $[{\rm L}]_0$ for $k_e > k_-$ where k_- is the unbinding rate of the ligand from the bound ground-state conformation of the protein (see Fig 1(b)). A decrease of the dominant relaxation rate $k_{\rm obs}$ with increasing ligand concentration $[{\rm L}]_0$ thus indicates conformational-selection binding [25]. However, an increase of $k_{\rm obs}$ with $[{\rm L}]_0$ under pseudo-first-order conditions is possible both for induced-fit binding and conformational-selection binding and does not uniquely point towards a binding mechanism [22].

In this article, we present general analytical results for the dominant relaxation rate $k_{\rm obs}$ of induced-fit binding and conformational-selection binding processes that hold for all ligand and protein concentrations. Our general results are based on an expansion of the rate equations for these binding processes around the equilibrium concentrations of ligands and proteins, and include the pseudo-first-order results in the limit of large ligand concentrations. In the case of induced-fit binding, we find that $k_{\rm obs}$ exhibits a minimum at the total ligand concentration $[{\rm L}]_0^{\rm min} = [{\rm P}]_0 - K_d$ for total protein concentrations $[{\rm P}]_0$ that are larger than the overall dissociation constant K_d of the binding process. As a characteristic feature, the function $k_{\rm obs}([{\rm L}]_0)$ for induced-fit binding is symmetric with respect to this minimum. At sufficiently large protein concentrations $[{\rm P}]_0$, the function $k_{\rm obs}([{\rm L}]_0)$ tends to identical values for small ligand concentrations $[{\rm L}]_0 \ll [{\rm P}]_0$ and for large ligand concentrations $[{\rm L}]_0 \gg [{\rm P}]_0$ because of its symmetry (see Fig 1(c)). In the case of conformational-selection binding, we find that $k_{\rm obs}$ exhibits a minimum for conformational excitation rates $k_e > k_-$ and sufficiently large protein concentrations $[{\rm P}]_0$ (see Fig 1(d)). The location $[{\rm L}]_0^{\rm min}$ of this minimum depends on $[{\rm P}]_0$, K_d, and the rates k_e and k_- (see Eq (10) below). In contrast to induced-fit binding, the function $k_{\rm obs}([{\rm L}]_0)$ for conformational-selection binding is not symmetric with respect to this minimum. At sufficiently large protein concentrations $[{\rm P}]_0$, the function $k_{\rm obs}([{\rm L}]_0)$ attains values for small ligand concentrations $[{\rm L}]_0 \ll [{\rm P}]_0$ that can greatly exceed the values for large ligand concentrations $[{\rm L}]_0 \gg [{\rm P}]_0$ (see Fig 1(d)). For excitation rates $k_e < k_-$ of conformational-selection binding processes, the dominant relaxation rate $k_{\rm obs}$ decreases monotonically with increasing ligand concentration $[{\rm L}]_0$ (see Fig 1(e)). Our general results for the dominant relaxation rate $k_{\rm obs}$ of induced-fit and conformational-selection binding processes allow to clearly distinguish between these two binding mechanisms for sufficiently large protein concentrations $[{\rm P}]_0$ (see Figs 2 and 3 below for numerical examples).

Results

Solving the rate equations of the induced-fit and conformational-selection binding models shown in Fig 1(a) and 1(b) is complicated by the fact that the binding steps in these models are second-order reactions that depend on the product of the time-dependent concentrations of unbound proteins and unbound ligands. In the standard pseudo-first-order approximation, the rate equations are simplified by assuming that the total ligand concentration greatly

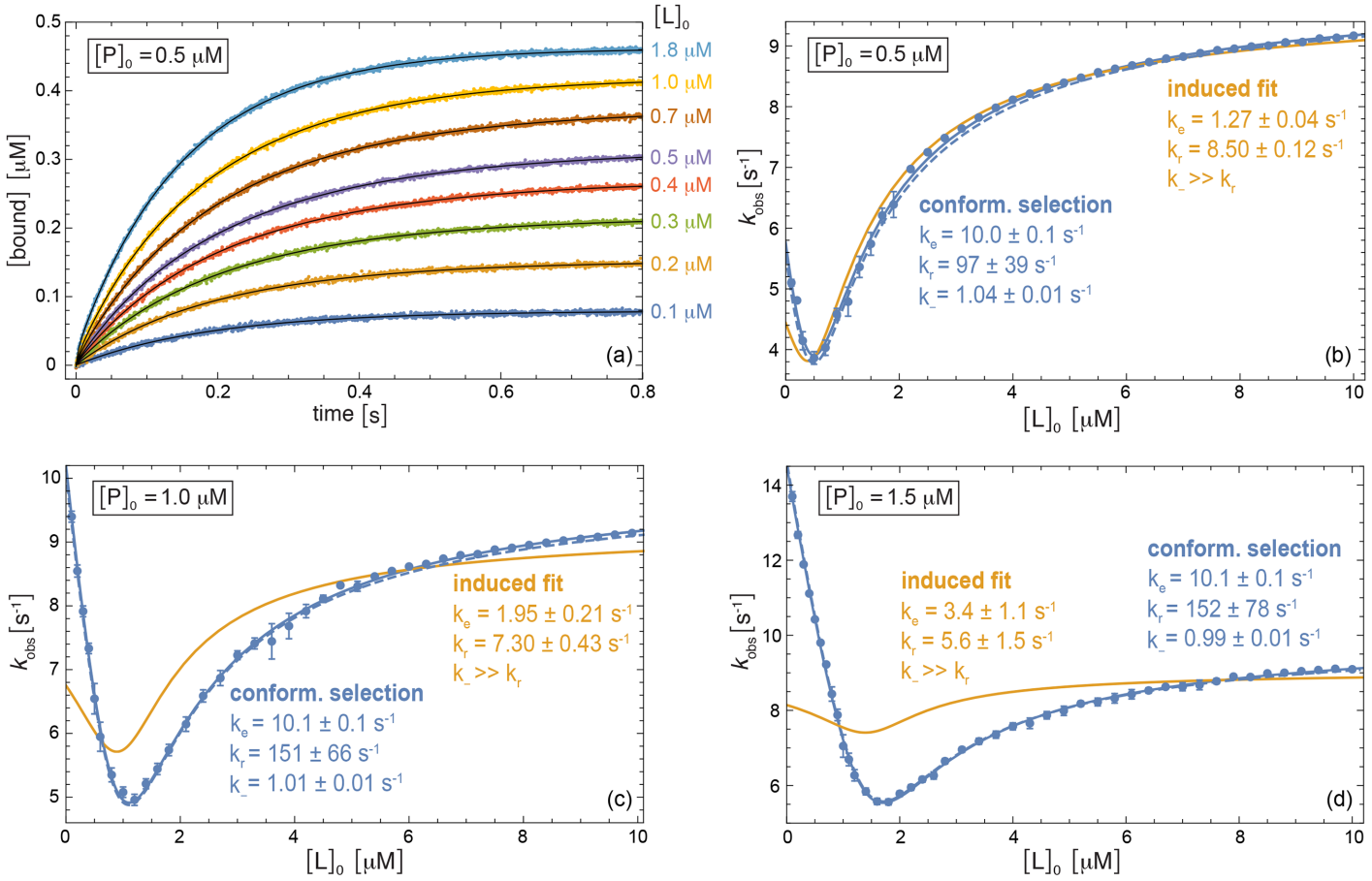

Fig 2. Numerical example for conformational-selection binding with the rate constants $k_e = 10\ s^{-1}$, $k_r = 100\ s^{-1}$, $k_+ = 100\ \mu M^{-1}s^{-1}$, and $k_- = 1\ s^{-1}$. (a) Relaxation data for the bound complex obtained by numerical integration of the rate equations and subsequent addition of Gaussian noise with amplitude 0.002 μM at the total protein concentration $[P]_0 = 0.5$ μM and exemplary total ligand concentrations $[L]_0$. The black lines represent multi-exponential fits of the data points. (b) to (d) Comparison of k_{obs} values obtained from multi-exponential fits of numerical relaxation data (points) to our theoretical results for k_{obs} (lines) at the three different total protein concentrations $[P]_0 = 0.5$ μM, 1.0 μM, and 1.5 μM and total ligand concentrations $[L]_0$ between 0.1 μM and 10 μM. The full lines represent fits of Eq (6) for conformational-selection binding (blue) and of Eq (1) for induced-fit binding (orange), with fit parameter values specified in the figure. In these fits, the dissociation constant $K_d = 0.11$ μM is assumed to be known from equilibrium data. The dashed blue lines are obtained from Eq (6) for the 'true' rate constants of the numerical example.

doi:10.1371/journal.pcbi.1005067.g002

exceeds the total protein concentration, so that the amount of ligand consumed during binding is negligible compared to the total amount of ligand. The concentration of the unbound ligand then can be taken to be constant, and the rate equations only contain terms that are linear in the time-dependent concentration of the protein, which makes them solvable. In our more general approach, a linearization of the rate equations is achieved by expanding around the equilibrium concentrations of the bound and unbound proteins and ligands (see Methods). This expansion captures the final relaxation into equilibrium, which is governed by the smallest, dominant relaxation rate k_{obs}, for all concentrations of proteins and ligands, and leads to general results for k_{obs} that include the results from the pseudo-first-order approximation in the limit of large ligand concentrations.

Dominant relaxation rate of induced-fit binding

Expanding the rate equations of the induced-fit binding mechanism shown in Fig 1(a) around the equilibrium concentrations of proteins and ligands leads to the dominant, smallest

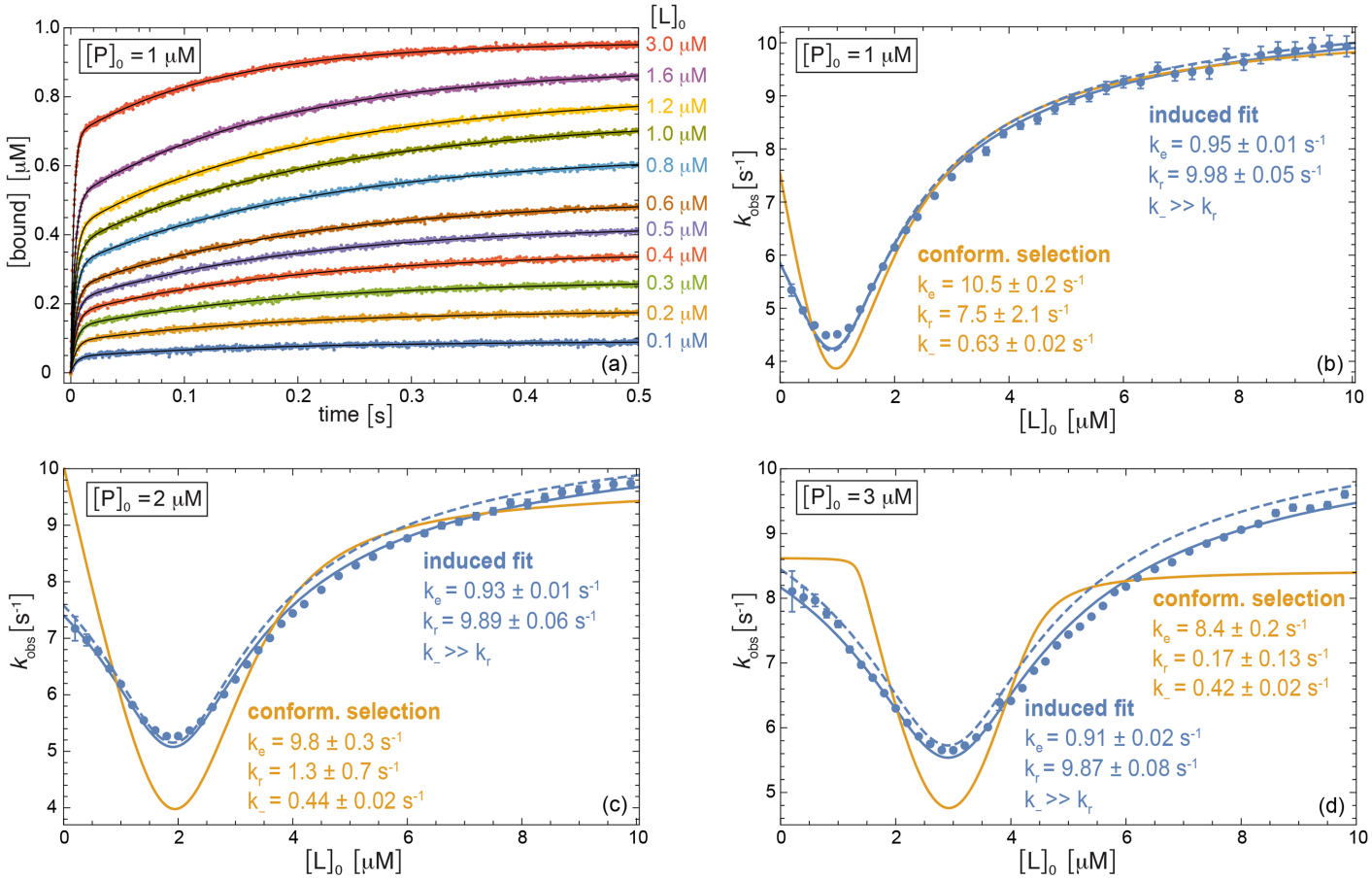

Fig 3. Numerical example for induced-fit binding with the rate constants $k_+ = 100\ \mu M^{-1}s^{-1}$, $k_- = 100\ s^{-1}$, $k_e = 1\ s^{-1}$, and $k_r = 10\ s^{-1}$. (a) Relaxation data for the bound complex obtained by numerical integration of the rate equations and subsequent addition of Gaussian noise with amplitude 0.004 μM at the total protein concentration $[P]_0 = 1$ μM and exemplary total ligand concentrations $[L]_0$. The black lines represent multi-exponential fits of the data points. (b) to (d) Comparison of k_{obs} values obtained from multi-exponential fits of numerical relaxation data (points) to our theoretical results for k_{obs} (lines) at the three different total protein concentrations $[P]_0 = 1$ μM, 2 μM, and 3 μM and total ligand concentrations $[L]_0$ between 0.1 μM and 10 μM. The full lines represent fits of Eq (1) for induced-fit binding (blue) and of Eq (6) for conformational-selection binding (orange), with fit parameter values specified in the figure. In these fits, the dissociation constant $K_d = 1/11$ μM is assumed to be known from equilibrium data. The dashed blue lines are obtained from Eq (1) for the 'true' rate constants of the numerical example.

doi:10.1371/journal.pcbi.1005067.g003

relaxation rate (see Methods)

$$k_{\mathrm{obs}} = k_e + k_r + \frac{1}{2}\gamma - \frac{1}{2}\sqrt{\gamma^2 + 4k_-k_r} \tag{1}$$

with

$$\gamma = -k_e - k_r + k_- + k_+(\delta - K_d) \tag{2}$$

$$\delta = \sqrt{\left([\mathrm{L}]_0 - [\mathrm{P}]_0 + K_d\right)^2 + 4[\mathrm{P}]_0K_d} \tag{3}$$

and with the overall dissociation constant

$$K_d = \frac{k_-k_e}{k_+(k_e + k_r)} \tag{4}$$

of induced-fit binding. This general result for k_{obs} holds for all total ligand concentrations $[L]_0$ and protein concentrations $[P]_0$. In the limit of large ligand concentrations $[L]_0 \gg [P]_0$, we obtain $\delta \simeq [L]_0 + K_d$ and $\gamma \simeq -k_e - k_r + k_- + k_+[L]_0$ from Eqs (2) and (3), which agrees with results derived in pseudo-first-order approximation [21, 22].

As a function of the total ligand concentration $[L]_0$, the dominant relaxation rate k_{obs} exhibits a minimum at

$$[L]_0^{min} = [P]_0 - K_d \tag{5}$$

for total protein concentrations $[P]_0 > K_d$. The function $k_{obs}([L]_0)$ is symmetric with respect to $[L]_0^{min}$ (see (Fig 1(c)). This symmetry and the location $[L]_0^{min}$ of the minimum result from the fact that k_{obs} depends on $[L]_0$ only via the term δ, which is minimal at $[L]_0^{min}$ and symmetric with respect to $[L]_0^{min}$. The dominant relaxation rate k_{obs} is minimal when δ is minimal. For large ligand concentrations $[L]_0$, k_{obs} tends towards the maximum value $k_e + k_r$ as in pseudo-first-order approximation. The location $[L]_0^{min}$ of the minimum and the symmetry of the function $k_{obs}([L]_0)$ with respect to this minimum are properties that the induced-fit binding model appears to 'inherit' from the elementary binding model $P + L \rightleftharpoons PL$ (see Eq (46) in Methods section). However, the function $k_{obs}([L]_0)$ of the elementary binding model is V-shaped and does not tend to a constant maximum value for large ligand concentrations $[L]_0$.

Dominant relaxation rate of conformational-selection binding

For the conformational-selection binding mechanism shown in Fig 1(b), an expansion of the rate equations around the equilibrium concentrations of proteins and ligands leads to the dominant, smallest relaxation rate (see Methods)

$$k_{obs} = k_e + \frac{1}{2}\alpha - \frac{1}{2}\sqrt{\alpha^2 + \beta} \tag{6}$$

with

$$\alpha = k_r - k_e + \frac{k_-\left((2k_e + k_r)\delta + k_r\left([L]_0 - [P]_0 - K_d\right)\right)}{2k_e K_d} \tag{7}$$

$$\beta = 2k_r\left(2k_e - k_- - \frac{k_-\left(\delta - [L]_0 + [P]_0\right)}{K_d}\right) \tag{8}$$

and δ as in Eq (3), and with the overall dissociation constant

$$K_d = \frac{k_-(k_e + k_r)}{k_+ k_e} \tag{9}$$

of conformational-selection binding. This general result for k_{obs} holds for all total ligand concentrations $[L]_0$ and protein concentrations $[P]_0$. In the limit of large ligand concentrations $[L]_0 \gg [P]_0$, we obtain $\alpha \simeq -k_e + k_r + k_- + k_+[L]_0$ and $\beta \simeq 4k_r(k_e - k_-)$ from Eqs (3), (7) and (8), in agreement with results derived in pseudo-first-order approximation [21, 22].

For conformational-selection binding, the shape of the function $k_{obs}([L]_0)$ depends on the values of the conformational excitation rate k_e and the unbinding rate k_- (see Fig 1(d) and 1(e)). For $k_e < k_-$, the dominant relaxation rate k_{obs} decreases monotonically with increasing total ligand concentration $[L]_0$. For $k_e > k_-$, the dominant relaxation rate k_{obs} exhibits a minimum as a function of $[L]_0$ at sufficiently large total protein concentrations $[P]_0$. The minimum

is located at (see Methods)

$$[\mathrm{L}]_0^{\min} \simeq \frac{k_e + k_-}{k_e - k_-}[\mathrm{P}]_0 - K_d \tag{10}$$

if the conformational relaxation rate k_r is much larger than the excitation rate k_e, which typically holds for the conformational exchange between ground-state and excited-state conformations of proteins. In contrast to induced-fit binding, the function $k_{\mathrm{obs}}([\mathrm{L}]_0)$ is not symmetric with respect to this minimum. For large ligand concentrations, the limiting value of the dominant relaxation rate is $k_{\mathrm{obs}}(\infty) = k_e$ as in pseudo-first-order approximation. For vanishing ligand concentrations $[\mathrm{L}]_0 \to 0$, the limiting value is $k_{\mathrm{obs}}(0) = k_e + k_r$ for total protein concentrations $[\mathrm{P}]_0 > K_d(k_e + k_r - k_-)/k_-$ and $k_{\mathrm{obs}}(0) = k_-([\mathrm{P}]_0 + K_d)/K_d$ for $[\mathrm{P}]_0 < K_d(k_e + k_r - k_-)/k_-$.

Distinguishing induced fit and conformational selection

The general results for the dominant relaxation rate k_{obs} presented in the previous sections allow to clearly distinguish induced-fit from conformational-selection binding processes. In Fig 2, we consider a conformational-selection binding process with the rate constants $k_e = 10\ \mathrm{s}^{-1}$, $k_r = 100\ \mathrm{s}^{-1}$, $k_+ = 100\ \mu\mathrm{M}^{-1}\mathrm{s}^{-1}$, and $k_- = 1\ \mathrm{s}^{-1}$ as a numerical example. The data points in Fig 2(a) represent relaxation curves for the bound complex that have been generated by numerical integration of the rate equations and subsequent addition of Gaussian noise to mimic measurement errors. The black lines in Fig 2(a) are multi-exponential fits of the data points. The number of exponentials in these fits has been determined with the Akaike information criterion (AIC), which is a standard criterion for the trade-off between quality of fit and number of fit parameters, and ranges from 2 to 4. The data points in Fig 2(b) to 2(d) represent the dominant relaxation rates k_{obs} that are obtained from multi-exponential fits of relaxation curves for different total ligand concentrations $[\mathrm{L}]_0$ and total protein concentrations $[\mathrm{P}]_0$. The dominant relaxation rate k_{obs} here is identified as the smallest relaxation rate of a multi-exponential fit. The full blue lines in Fig 2(b) to 2(d) result from fitting our general result Eq (6) for conformational-selection binding to the k_{obs} data points. The full orange lines represent fits of our general result Eq (1) for induced-fit binding. For all fits, we assume that the dissociation constant $K_d = 0.11\ \mu\mathrm{M}$ is known from equilibrium data, and use k_e, k_r, and k_- as fit parameters. Finally, the blue dashed lines in Fig 2(b) to 2(d) are the k_{obs} curves obtained from Eq (6) for the 'true' rate constants of the conformational-selection binding process given above. These dashed lines agree with the data points, which indicates that the k_{obs} values from multi-exponential fits as in Fig 2(a) are identical to the values obtained from Eq (6) within the statistical errors of the numerical example.

The fits in Fig 2(b) to 2(d) clearly identify conformational selection as the correct binding mechanism in this example. The blue fit curves for conformational selection agree with the data points within statistical errors, while the orange fit curves for induced fit deviate from the data. For conformational-selection binding, the fit values of the conformational transition rates k_e and k_r and of the unbinding rate k_- specified in the figure agree with the correct values $k_e = 10\ \mathrm{s}^{-1}$, $k_r = 100\ \mathrm{s}^{-1}$, and $k_- = 1\ \mathrm{s}^{-1}$ of the numerical example within statistical errors.

In Fig 3, we consider an induced-fit binding process with rate constants $k_+ = 100\ \mu\mathrm{M}^{-1}\mathrm{s}^{-1}$, $k_- = 100\ \mathrm{s}^{-1}$, $k_e = 1\ \mathrm{s}^{-1}$, and $k_r = 10\ \mathrm{s}^{-1}$ as a second numerical example. The k_{obs} data points in Fig 3(b) to 3(d) are again obtained from multi-exponential fits of relaxation curves that have been generated by numerical integration of the rate equations and subsequent addition of Gaussian noise (see Fig 3(a)). The fits in Fig 3(b) to 3(d) clearly identify induced-fit binding as the correct mechanism in this example. The full blue curves that represent fits of Eq (1) for induced-fit binding are in overall agreement with the k_{obs} points, while the orange fit curves of

Eq (6) for conformational-selection binding deviate from the data. The fit values of the conformational transition rates k_e and k_r for the induced-fit binding model are in good agreement with the correct values $k_e = 1\ s^{-1}$, and $k_r = 10\ s^{-1}$ of the example. The dashed blue curves in Fig 3(b) to 3(d), which are obtained from Eq (1) for the 'true' rate constants of the induced-fit binding process, are in overall agreement with the data points. Slight deviations result from the fact that the amplitude of the slow relaxation mode with rate k_{obs} is rather small compared to the amplitude of the fast modes (see Fig 3(a)), which can lead to numerical inaccuracies.

In both numerical examples of Figs 2 and 3, the correct binding mechanism cannot be identified under pseudo-first-order conditions because k_{obs} is monotonically increasing with $[L]_0$ for ligand concentrations that greatly exceed the protein concentration $[P]_0$ [22].

Analysis of chemical relaxation rates for recoverin binding

Chakrabarti et al. [28] have recently investigated the conformational dynamics and binding kinetics of the protein recoverin with chemical relaxation and advanced NMR experiments. Recoverin exhibits a conformational change during binding of its ligand, which is a rhodopsin kinase peptide fused to the B1 domain of immunoglobulin protein G in the experiments of Chakrabarti et al. [28]. The data points in Fig 4 represent the dominant relaxation rates k_{obs} obtained by Chakrabarti et al. from relaxation experiments at the temperatures 30°C and 10°C for a recoverin concentration of 10μM. The lines in Fig 4 result from fitting our general results Eqs (1) and (6) for the dominant relaxation rate k_{obs} of induced-fit and conformational-selection binding processes. In these fits, we have used the values $K_d = 1.0 \pm 0.2$ μM and $K_d = 1.8 \pm 0.2$ μM obtained by Chakrabarti et al. from isothermal titration calometry experiments at 30°C and 10°C, which reduces the parameters to k_e, k_r, and k_-. The fits of our general result Eq (6) for conformational-selection binding are rather insensitive to the relaxation rate k_r, which is illustrated in Fig 4 by nearly identical fits for $k_r = 100\ s^{-1}$ and $k_r = 1000\ s^{-1}$

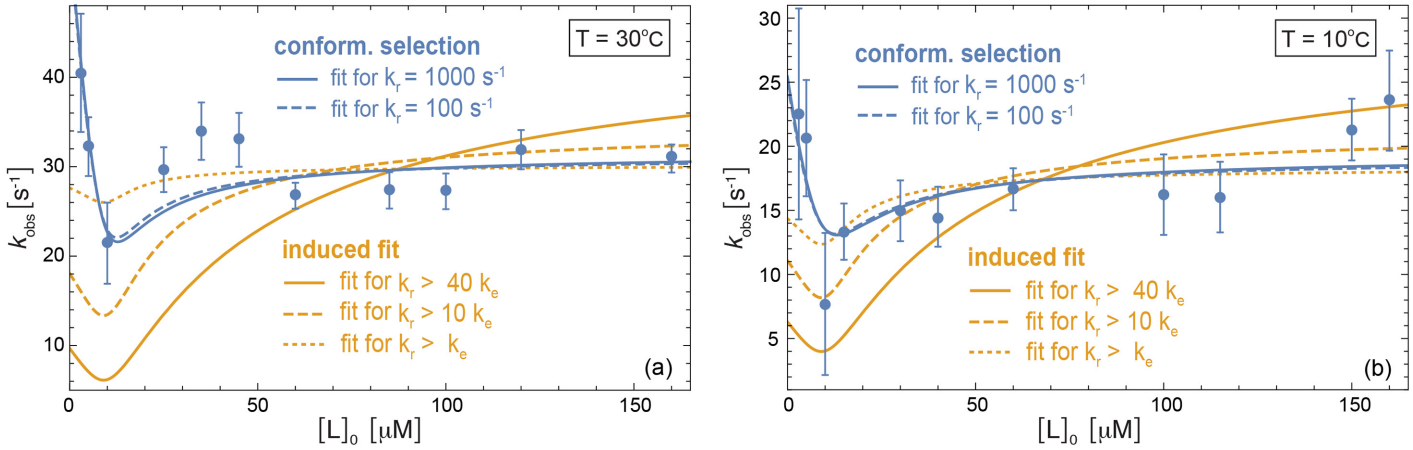

Fig 4. Analysis of experimentally determined relaxation rates k_{obs} for the binding of recoverin to a rhodopsin kinase peptide ligand. The data points represent results of Chakrabarti et al. [28] obtained from chemical relaxation experiments at the temperatures 30°C and 10°C for a recoverin concentration of 10 μM. The blue lines result from fits of Eq (6) for conformational-selection binding with the values $k_r = 1000\ s^{-1}$ (full) and $k_r = 100\ s^{-1}$ (dashed) of the conformational relaxation rate. At 30°C, the parameter values obtained from fitting are $k_e = 31.5 \pm 0.8\ s^{-1}$ and $k_- = 5.1 \pm 0.4\ s^{-1}$ for $k_r = 1000\ s^{-1}$, and $k_e = 31.1 \pm 0.8\ s^{-1}$ and $k_- = 5.0 \pm 0.4\ s^{-1}$ for $k_r = 100\ s^{-1}$. At 10°C, the fit parameter values are $k_e = 19.3 \pm 1.4\ s^{-1}$ and $k_- = 3.9 \pm 0.7\ s^{-1}$ for $k_r = 1000\ s^{-1}$, and $k_e = 19.0 \pm 1.3\ s^{-1}$ and $k_- = 3.8 \pm 0.7\ s^{-1}$ for $k_r = 100 s^{-1}$. The yellow lines represent fits of Eq (1) for induced-fit binding with constraints on the conformational excitation and relaxation rates k_e and k_r. At 30°C, the obtained fit values for the conformational exchange rates are $k_e = k_r = 15 \pm 10\ s^{-1}$ for the constraint $k_r > k_e$, $k_e = 3.1 \pm 1.9\ s^{-1}$ and $k_r = 31 \pm 4 s^{-1}$ for the constraint $k_r > 10k_e$, and $k_e = 1.1 \pm 0.8\ s^{-1}$ and $k_r = 44 \pm 8\ s^{-1}$ for $k_r > 40k_e$. At 10°C, the fit values are $k_e = 4.5 \pm 4.0\ s^{-1}$ and $k_r = 14 \pm 10\ s^{-1}$ for the constraint $k_r > k_e$, $k_e = 1.9 \pm 1.5\ s^{-1}$ and $k_r = 19 \pm 5\ s^{-1}$ for $k_r > 10k_e$, and $k_e = 0.7 \pm 0.5\ s^{-1}$ and $k_r = 28 \pm 11\ s^{-1}$ for $k_r > 40k_e$. In all fits of Eq (1) for induced-fit binding, we obtain $k_- \gg k_r$, i.e. the fit values of the unbinding rate k_- are much larger than the conformational relaxation rate k_r and cannot be specified.

doi:10.1371/journal.pcbi.1005067.g004

(see dashed and full blue lines). Our fit values for the conformational excitation rate k_e specified in the figure caption agree with the values $k_e = 33 \pm 5\ s^{-1}$ and $k_e = 23 \pm 5\ s^{-1}$ obtained by Chakrabarti et al. from advanced NMR experiments at 30°C and 10°C, respectively. From these experiments, Chakrabarti et al. obtain the values $k_r = 990 \pm 100\ s^{-1}$ and $k_r = 920 \pm 200\ s^{-1}$ at 30°C and 10°C, which cannot be deduced from our fits of the k_{obs} data because these fits are insensitive to k_r. The NMR experiments indicate that the higher-energy conformation of unbound recoverin resembles the ground-state conformation of bound recoverin [28] as required for the conformational-selection binding mechanism illustrated in Fig 1(b), and that the excited-state conformation of unbound recoverin has the equilibrium occupancy $P_e = k_e/(k_r + k_e) = 3.2\% \pm 0.5\%$ at 30°C and $P_e = 2.4\% \pm 0.7\%$ at 10°C, relative to the ground-state conformation.

Fits of our general result Eq (1) for the dominant relaxation rate k_{obs} of induced-fit binding with unconstrained parameters k_e, k_r, and k_- lead to fit values for the conformational exchange rates k_e and k_r with $k_e \gg k_r$. For such values of k_e and k_r, the conformation 1 of the induced-fit binding model illustrated in Fig 1(a) is the ground-state conformation both for the unbound state and the bound state of recoverin, which contradicts the experimental observation that recoverin changes its conformation during binding [28]. Distinct ground-state conformations for the unbound and bound state of recoverin can be enforced by constraining k_r to values larger than k_e. The yellow lines in Fig 4 result from fits with the constraints $k_r > k_e$, $k_r > 10k_e$, and $k_r > 40k_e$. These constraints correspond to equilibrium occupancies P_e of the excited-state conformation of bound recoverin with $P_e < 50\%$, $P_e < 9.1\%$, and $P_e < 2.4\%$, respectively. The fits of Eq (1) for induced-fit binding with the constraints $k_r > 10k_e$ and $k_r > 40k_e$ deviate rather strongly from the two data points with the smallest ligand concentrations $[L]_0 = 3\ \mu M$ and $5\ \mu M$, in contrast to fits of Eq (6) for conformational-selection binding (blue lines). A Bayesian model comparison of conformational-selection binding and induced-fit binding based on Eqs (1) and (6) leads to Bayes factors of $9.8 \cdot 10^{13}$ and $1.5 \cdot 10^{23}$ at 30°C for the constraints $k_r > 10k_e$ and $k_r > 40k_e$, and to Bayes factors of $4.2 \cdot 10^3$ and $9.6 \cdot 10^9$ at 10°C for $k_r > 10k_e$, and $k_r > 40k_e$, respectively (see Methods for details). These Bayes factors indicate that the k_{obs} data of Fig 4 strongly point towards conformational-selection binding. Bayes factors larger than 10^2 are generally considered to be decisive [37]. For the bound recoverin complex, Chakrabarti et al. did not observe an excited-state conformation in NMR experiments, which limits the excited-state occupancy P_e to undetectable values smaller than 1% for a conformational exchange that is fast compared to the NMR timescale as in the case of unbound recoverin. The analysis of the experimental data for the dominant relaxation rate k_{obs} of recoverin binding based on our general results Eqs (1) and (6) thus indicates a conformational-selection binding mechanism, in agreement with a numerical analysis of Chakrabarti et al. [28]. In this numerical analysis, Chakrabarti et al. include the chemical relaxation data for recoverin binding, additional relaxation data from dilution experiments, the values for the conformational exchange rates k_e and k_r obtained from NMR experiments, and the K_d values deduced from isothermal titration calometry [28]. In contrast, our analysis of the k_{obs} data in Fig 4 from the chemical relaxation experiments of recoverin binding only includes the K_d values from isothermal titration calometry as additional input.

Discussion

We have shown here that the dominant rate k_{obs} of chemical relaxation experiments with total protein and ligand concentrations of comparable magnitude conveys information on the binding mechanism and conformational transition rates of proteins. For sufficiently large protein concentrations $[P]_0$, the function $k_{obs}([L]_0)$ obtained from such experiments has characteristic

features that are clearly distinct for induced-fit binding and conformational-selection binding. The function $k_{obs}([L]_0)$ of induced-fit binding exhibits a characteristic symmetry around a minimum and tends to identical values for small and large ligand concentrations $[L]_0$ as in Fig 1(c) if the protein concentration $[P]_0$, which determines the location of the minimum, is sufficiently large. In contrast, the function $k_{obs}([L]_0)$ of conformational-selection binding is either monotonically decreasing for $k_e < k_-$, or asymmetric around a minimum for $k_e > k_-$. In both cases, $k_{obs}([L]_0)$ tends for small ligand concentrations $[L]_0$ to values that exceed the values for large ligand concentrations as in Fig 1(d) and 1(e) if the protein concentration $[P]_0$ is sufficiently large.

Our general results for the dominant rate k_{obs} of chemical relaxation experiments thus provide a transparent route to distinguish induced-fit binding from conformational-selection binding based on the shape of the function $k_{obs}([L]_0)$, and to infer conformational transition rates from fitting. Alternatively, these binding mechanisms can be identified from a numerical analysis of time-dependent relaxation curves [26–28], based on steric effects that may prohibit ligand entry and exit in the bound ground-state conformation of the protein and, thus, rule out conformational-selection binding [15], from a comparison of conformational excitation rates to overall, effective binding and unbinding rates [4, 13], or from the effect of distal mutations that mainly affect the conformational exchange, but not the binding kinetics in different protein conformations [13, 16, 21, 38]. Of particular interest is how such mutations change the overall binding and unbinding rates. If both conformational-selection and induced-fit binding are viable, increasing the ligand concentration may shift the binding mechanism from conformational selection to induced fit [16, 18, 26, 39, 40].

Methods

Near-equilibrium relaxation of induced-fit binding

The induced-fit binding model of Fig 1(a) leads to the four rate equations

$$\frac{\mathrm{d}}{\mathrm{d}t}[P_1] = -k_+[P_1][L] + k_-[P_1L] \tag{11}$$

$$\frac{\mathrm{d}}{\mathrm{d}t}[L] = -k_+[P_1][L] + k_-[P_1L] \tag{12}$$

$$\frac{\mathrm{d}}{\mathrm{d}t}[P_1L] = k_+[P_1][L] - k_-[P_1L] + k_e[P_2L] - k_r[P_1L] \tag{13}$$

$$\frac{\mathrm{d}}{\mathrm{d}t}[P_2L] = k_r[P_1L] - k_e[P_2L] \tag{14}$$

that describe the time-dependent evolution of the concentration $[P_1]$ of the unbound protein, the concentration $[L]$ of the unbound ligand, and the concentrations $[P_1L]$ and $[P_2L]$ of the bound complexes. These four rate equations are redundant because the total concentrations $[P]_0$ and $[L]_0$ of proteins and ligands are conserved:

$$[P_1L] + [P_2L] + [P_1] = [P]_0 \tag{15}$$

$$[L] + [P_1L] + [P_2L] = [L]_0 \tag{16}$$

With Eqs (15) and (16), the concentrations $[P_1]$ and $[P_1L]$ can be expressed in terms of $[L]$ and

$[P_2L]$, which results in the two non-redundant rate equations

$$\frac{d}{dt}[L] = -k_+([L] - [L]_0 + [P]_0)[L] + k_-([L]_0 - [L] - [P_2L]) \tag{17}$$

$$\frac{d}{dt}[P_2L] = k_r([L]_0 - [L] - [P_2L]) - k_e[P_2L] \tag{18}$$

These rate equations can be written in the vectorial form

$$\frac{d}{dt}\mathbf{c} = \mathbf{F}(\mathbf{c}) \tag{19}$$

with

$$\mathbf{c}(t) \equiv \begin{pmatrix} [L](t) \\ [P_2L](t) \end{pmatrix} \tag{20}$$

The two components of the vector $\mathbf{F}(\mathbf{c})$ in Eq (19) are the right-hand sides of the Eqs (17) and (18). The rate equations describe the temporal evolution of the concentrations [L] and $[P_2L]$ towards equilibrium, and are nonlinear because of the quadratic term in [L] on the right-hand side of Eq (17).

To obtain linearized versions of the rate equations that describe the slow processes corresponding to the final relaxation into equilibrium, we expand the vector $\mathbf{F}(\mathbf{c})$ in Eq (19) around the equilibrium concentrations $\mathbf{c}_{eq}$:

$$\mathbf{F}(\mathbf{c}) = \mathbf{F}(\mathbf{c}_{eq} + \Delta\mathbf{c}) \simeq \mathbf{F}(\mathbf{c}_{eq}) + J(\mathbf{c}_{eq})\Delta\mathbf{c} = J(\mathbf{c}_{eq})\Delta\mathbf{c} \tag{21}$$

Here, J is the Jacobian matrix of $\mathbf{F}$ with elements $J_{ij} = \partial F_i/\partial c_j$. The right-hand side of Eq (21) follows from $\mathbf{F}(\mathbf{c}_{eq}) = 0$. Inserting the expansion (21) into Eq (19) and making use of $\frac{d}{dt}\mathbf{c} = \frac{d}{dt}(\mathbf{c}_{eq} + \Delta\mathbf{c}) = \frac{d}{dt}\Delta\mathbf{c}$ leads to the linearized rate equations

$$\frac{d}{dt}\Delta\mathbf{c} = J(\mathbf{c}_{eq})\Delta\mathbf{c} \tag{22}$$

with

$$J(\mathbf{c}_{eq}) = \begin{pmatrix} k_+\left([L]_0 - 2[L]_{eq} - [P]_0\right) - k_- & -k_- \\ -k_r & -k_e - k_r \end{pmatrix} \tag{23}$$

and the equilibrium concentration of the unbound ligand

$$[L]_{eq} = \frac{1}{2}\left([L]_0 - [P]_0 - K_d + \sqrt{\left([L]_0 - [P]_0 + K_d\right)^2 + 4[P]_0K_d}\right) \tag{24}$$

The overall dissociation constant K_d of the induced-fit binding process is given in Eq (4). The relaxation rates of the linearized rate Eq (22) are the two eigenvalues of the matrix $-J(\mathbf{c}_{eq})$. These eigenvalues are k_{obs} given in Eq (1) and

$$k_2 = k_e + k_r + \frac{1}{2}\gamma + \frac{1}{2}\sqrt{\gamma^2 + 4k_-k_r} \tag{25}$$

with γ and δ given in Eqs (2) and (3). The relaxation rate k_{obs} is smaller than k_2 and, thus, dominates the final relaxation into equilibrium.

Near-equilibrium relaxation of conformational-selection binding

The four rate equations of the conformational-selection binding model of Fig 1(b) are

$$\frac{\mathrm{d}}{\mathrm{d}t}[\mathrm{P}_1] = -k_e[\mathrm{P}_1] + k_r[\mathrm{P}_2] \tag{26}$$

$$\frac{\mathrm{d}}{\mathrm{d}t}[\mathrm{P}_2] = k_e[\mathrm{P}_1] - k_r[\mathrm{P}_2] + k_-[\mathrm{P}_2\mathrm{L}] - k_+[\mathrm{P}_2][\mathrm{L}] \tag{27}$$

$$\frac{\mathrm{d}}{\mathrm{d}t}[\mathrm{L}] = k_-[\mathrm{P}_2\mathrm{L}] - k_+[\mathrm{P}_2][\mathrm{L}] \tag{28}$$

$$\frac{\mathrm{d}}{\mathrm{d}t}[\mathrm{P}_2\mathrm{L}] = -k_-[\mathrm{P}_2\mathrm{L}] + k_+[\mathrm{P}_2][\mathrm{L}] \tag{29}$$

The total concentrations $[\mathrm{L}]_0$ and $[\mathrm{P}]_0$ of the ligands and proteins are conserved:

$$[\mathrm{L}] + [\mathrm{P}_2\mathrm{L}] = [\mathrm{L}]_0 \tag{30}$$

$$[\mathrm{P}_1] + [\mathrm{P}_2] + [\mathrm{P}_2\mathrm{L}] = [\mathrm{P}]_0 \tag{31}$$

With these equations, the concentrations $[\mathrm{P}_1]$ and $[\mathrm{P}_2\mathrm{L}]$ can be expressed in terms of $[\mathrm{L}]$ and $[\mathrm{P}_2]$, which leads to the two rate equations

$$\frac{\mathrm{d}}{\mathrm{d}t}[\mathrm{P}_2] = k_e\big([\mathrm{P}]_0 - [\mathrm{P}_2]\big) - (k_r + k_+[\mathrm{L}])[\mathrm{P}_2] + (k_- - k_e)([\mathrm{L}]_0 - [\mathrm{L}]) \tag{32}$$

$$\frac{\mathrm{d}}{\mathrm{d}t}[\mathrm{L}] = k_-([\mathrm{L}]_0 - [\mathrm{L}]) - k_+[\mathrm{P}_2][\mathrm{L}] \tag{33}$$

These rate equations can be written in the vectorial form of Eq (19) with

$$\mathbf{c}(t) \equiv \begin{pmatrix} [\mathrm{P}_2](t) \\ [\mathrm{L}](t) \end{pmatrix} \tag{34}$$

and with a vector $\mathbf{F}(\mathbf{c})$ that contains the right-hand sides of the Eqs (32) and (33) as components. An expansion of the vector $\mathbf{F}(\mathbf{c})$ around the equilibrium concentrations $\mathbf{c}_{\mathrm{eq}}$ leads to Eq (22) with the Jacobian matrix

$$J(\mathbf{c}_{\mathrm{eq}}) = -\begin{pmatrix} k_r + k_e + k_+[\mathrm{L}]_{\mathrm{eq}} & -k_e + k_- + k_+[\mathrm{P}_2]_{\mathrm{eq}} \\ k_+[\mathrm{L}]_{\mathrm{eq}} & k_- + k_+[\mathrm{P}_2]_{\mathrm{eq}} \end{pmatrix} \tag{35}$$

and the equilibrium concentrations

$$[\mathrm{P}_2]_{\mathrm{eq}} = \frac{1}{2K_d}\frac{k_-}{k_+}\left([\mathrm{P}]_0 - [\mathrm{L}]_0 - K_d + \sqrt{([\mathrm{P}]_0 - [\mathrm{L}]_0 - K_d)^2 + 4K_d[\mathrm{P}]_0}\right) \tag{36}$$

$$[\mathrm{L}]_{\mathrm{eq}} = \frac{1}{2}\left([\mathrm{L}]_0 - [\mathrm{P}]_0 - K_d + \sqrt{([\mathrm{P}]_0 - [\mathrm{L}]_0 - K_d)^2 + 4K_d[\mathrm{P}]_0}\right) \tag{37}$$

The overall dissociation constant K_d of the conformational-selection binding process is given in Eq (9). The relaxation rates of the linearized rate equations are the two eigenvalues of the

matrix $-J(\mathbf{c}_{eq})$. These eigenvalues are k_{obs} given in Eq (6) and

$$k_2 = k_e + \frac{1}{2}\alpha + \frac{1}{2}\sqrt{\alpha^2+\beta} \tag{38}$$

with α and β given in Eqs (7) and (8). The relaxation rate k_{obs} is smaller than k_2 and therefore dominates the final relaxation into equilibrium.

To derive Eq (10) for the location of the minimum of k_{obs} as a function of the total ligand concentration $[L]_0$, we now consider the near-equilibrium relaxation of the conformational-selection model in quasi-steady-state approximation (qssa), which assumes that the concentration of the intermediate $[P_2]$ does not change in time. The left-hand side of Eq (32) then is equal to zero, and the two Eqs (32) and (33) reduce to the single equation

$$\frac{d}{dt}[L] = -k_e k_- \frac{([L]+K_d)([L]-[L]_0)+[L][P]_0}{k_-[L]+k_e K_d} = f([L]) \tag{39}$$

An expansion of the function $f([L])$ around the equilibrium concentration $[L]_{eq}$ leads to the linear equation $d[L]/dt \simeq -k_{obs}^{(qssa)}([L]-[L]_{eq})$ with

$$k_{obs}^{(qssa)} = -\left.\frac{df([L])}{d[L]}\right|_{[L]=[L]_{eq}} = \frac{k_- k_e \delta}{k_e K_d + k_-[L]_{eq}} \tag{40}$$

and δ and $[L]_{eq}$ given in Eqs (3) and (37). The derivative of $k_{obs}^{(qssa)}$ is zero at $[L]_0 = [L]_0^{min}$ with $[L]_0^{min}$ given in Eq (10). In general, the quasi-steady-state result $k_{obs}^{(qssa)}$ is a good approximation of k_{obs} if the rates for the transitions out of the intermediate state P_2 of conformational-selection binding are much larger than the rates for the transitions to P_2. A numerical analysis shows that the location $[L]_0^{min}$ of the minimum of $k_{obs}^{(qssa)}([L])$ is in good agreement with the location of the minimum of $k_{obs}([L])$ for conformational transitions rates with $k_r \gg k_e$.

Multi-exponential relaxation

In the numerical examples illustrated in Figs 2 and 3, chemical relaxation curves for conformational-selection and induced-fit binding are fitted with a multi-exponential model. Such multi-exponential models are an adequate description for the time evolution of concentrations in first-order chemical reactions. However, the binding steps of the induced-fit and conformational-selection models of Fig 1(a) and 1(b) are of second order. To justify that multi-exponential models can also be used to approximate the chemical relaxation of second-order reactions, we consider here the elementary binding model

$$P + L \underset{k_-}{\overset{k_+[P][L]}{\rightleftharpoons}} PL \tag{41}$$

of a protein P and ligand L. For the initial condition $[PL](0) = 0$, the rate equation of the elementary binding model can be written as

$$\frac{d}{dt}[PL] = k_+([P]_0 - [PL])([L]_0 - [PL]) - k_-[PL] \tag{42}$$

and has the analytical solution [38]

$$[PL](t) = -\frac{\lambda_1(e^{(\lambda_1-\lambda_2)t}-1)}{k_+(e^{(\lambda_1-\lambda_2)t} - \lambda_1/\lambda_2)} \tag{43}$$

with

$$\lambda_{1,2} = -\frac{1}{2}k_+\left([\mathrm{P}]_0 + [\mathrm{L}]_0 + K_d \pm \sqrt{\left([\mathrm{P}]_0 + [\mathrm{L}]_0 + K_d\right)^2 - 4[\mathrm{P}]_0[\mathrm{L}]_0}\right) \tag{44}$$

where $K_d = k_-/k_+$ is the dissociation constant of the elementary binding model.

We first show that $\lambda_2 - \lambda_1$ is identical to the dominant relaxation rate k_{obs} obtained from a linear expansion around equilibrium. An expansion of the right-hand side of Eq (42) around the equilibrium concentration

$$[\mathrm{PL}]_{\mathrm{eq}} = \frac{1}{2}\left([\mathrm{P}]_0 + [\mathrm{L}]_0 + K_d - \sqrt{\left([\mathrm{L}]_0 - [P]_0 + K_d\right)^2 + 4K_d[P]_0}\right) \tag{45}$$

leads to the linear equation $\mathrm{d}[\mathrm{PL}]/\mathrm{d}t \simeq -k_{\mathrm{obs}}([\mathrm{PL}] - [\mathrm{PL}]_{\mathrm{eq}})$ with

$$k_{\mathrm{obs}} = k_+\sqrt{\left([\mathrm{L}]_0 - [P]_0 + K_d\right)^2 + 4K_d[P]_0} \tag{46}$$

This dominant relaxation rate k_{obs} is identical to $\lambda_2 - \lambda_1$. As a function of $[\mathrm{L}]_0$, the dominant rate k_{obs} of the elementary binding model exhibits a minimum at $[\mathrm{L}]_0^{\min} = [P]_0 - K_d$ and is symmetric with respect to this minimum.

We next use the limit of the geometric series $\sum_{n=0}^{\infty} q^n = 1/(1-q)$ with $q = e^{-k_{obs}\,t}\,\lambda_2/\lambda_1$ to rewrite Eq (43) as

$$[\mathrm{PL}](t) \propto \lambda_2 + (\lambda_2 - \lambda_1)\sum_{n=1}^{\infty}\frac{\mathrm{e}^{-nk_{\mathrm{obs}}t}}{(\lambda_1/\lambda_2)^n} \tag{47}$$

which shows that the chemical relaxation of the elementary binding model can be described as an infinite sum of exponential functions. The exponents of these functions are integer multiples of k_{obs}, which is reminiscent of the higher harmonics in oscillatory phenomena. The prefactors $(\lambda_2/\lambda_1)^n$ in Eq (47) decay exponentially with the order n of the harmonic because of $\lambda_2/\lambda_1 < 1$. The infinite sum of Eq (47) therefore can be truncated in practical situations. Under pseudo-first-order conditions, Eq (47) reduces to a single-exponential relaxation.

In analogy to the elementary binding model, we propose that the time evolution of the concentrations in the induced-fit and conformational-selection models can be represented as a sum of exponentials where the exponents are integer combinations $-ik_{\mathrm{obs}} - jk_2$ with $i, j = 0, 1, 2, 3, \ldots$ of the relaxation rates k_{obs} and k_2 obtained from a linear expansion around the equilibrium concentrations. Under pseudo-first-order conditions, the chemical relaxation reduces to a double-exponential relaxation [16, 21, 22].

In the numerical examples of Figs 2 and 3, the chemical relaxation of the bound complexes is fitted with a multi-exponential model

$$[\mathrm{bound}](t) = A_0 + \sum_{n=1}^{N} A_n e^{-k_n t} \tag{48}$$

with $k_n > 0$ for all n. We have used the routine NonlinearModelFit of the software Mathematica [41] with the differential evolution algorithm [42], which was repeatedly run with different values of its F parameter ranging from 0.1 to 1 for a given number of exponentials N. Among different runs, we have selected fit results based on the residual sum of squares, after discarding fits with singular results in which two rates k_n coincide within 95% confidence intervals, or in which one or more rates k_n are identical to 0 within 95% confidence intervals. We have then determined the number of exponentials N based on the small-sample-size corrected version of Akaike's information criterion (AIC) [43].

Bayes factors

The Bayes factor K is as measure for how plausible one model is relatively to an alternative model, given experimental data [44]. The Bayes factor for the plausibility of the conformational-selection binding model relative to induced-fit binding model is

$$K = \frac{\int p(\text{data} \mid \text{conformational} - \text{selection binding}, \theta) p(\theta) \mathrm{d}\theta}{\int p(\text{data} \mid \text{induced} - \text{fit binding}, \theta) p(\theta) \mathrm{d}\theta} \tag{49}$$

Here, $p(\text{data} \mid M, \theta)$ is the probability that the data were produced by the model M with given parameters θ, where M either stands for conformational-selection binding or induced-fit binding, and $p(\theta)$ is the prior distribution on the parameter values, which encodes any prior knowledge that we have about the parameters. The integrals of Eq (49) are taken over all parameter values and result in the probability $p(\text{data} \mid M)$ that the data were produced by the model, regardless of specific parameter values. The data here consist of the slowest relaxation rates $k_{\text{obs}}^{(i)}$ with $i = 1, 2, \ldots, N$ obtained from multi-exponential fits of the N time series with ligand concentrations $[L]_0^{(i)}$, and the errors σ_i of these rates. Following standard approaches [44], the probability that the data were generated by the model M with parameters $\theta = (k_e, k_r, k_-, K_d, [P]_0)$ is

$$p(\text{data} \mid M, \theta) \propto \prod_{i=1}^{N} \exp\left[-\frac{\left(k_{\text{obs}}^{(i)} - k_{\text{obs}}^{M}\left(\theta, [L]_0^{(i)}\right)\right)^2}{2\sigma_i^2} \right] \tag{50}$$

for $k_r > nk_e$, and 0 otherwise. The inequality $k_r > nk_e$ reflects constraints on the conformational relaxation rate k_r and excitation rate k_e of the models (see section "Analysis of chemical relaxation rates for recoverin binding"). Eq (50) implies that the errors $k_{\text{obs}}^{(i)} - k_{\text{obs}}^{M}(\theta, [L]_0^{(i)})$ are independently and normally distributed random variables with standard deviations σ_i. Depending on the model M, we either use Eqs (1) or (6) to determine $k_{\text{obs}}^{M}(\theta, [L]_0^{(i)})$. For simplicity, K_d and $[P]_0$ are kept fixed at the experimentally measured values. We choose a prior $p(\theta)$ that is uniform in the logarithm of the rates k_e, k_r, k_-. Taking the logarithm of the rates is not crucial, as a uniform prior on the rates gives similar results in the analysis of recoverin binding and, thus, leads to the same conclusions. The prior $p(\theta)$ here can be chosen to be uniform because it is identical for both the induced-fit and conformational-selection binding models due to the equivalent parameters of the models [45].

Acknowledgments

F. P. would like to thank Christof Schütte for insightful discussions.

Author Contributions

Analyzed the data: FP TRW.

Wrote the paper: FP TRW.

Conceived and designed the theory: FP TRW.

Performed the numerical analysis: FP TRW.

References

1. Gerstein M, Krebs W. A database of macromolecular motions. Nucleic Acids Res. 1998; 26:4280–4290. doi: 10.1093/nar/26.18.4280 PMID: 9722650

2. Eisenmesser EZ, Millet O, Labeikovsky W, Korzhnev DM, Wolf-Watz M, Bosco DA, et al. Intrinsic dynamics of an enzyme underlies catalysis. Nature. 2005; 438:117–121. doi: 10.1038/nature04105 PMID: 16267559
3. Beach H, Cole R, Gill M, Loria J. Conservation of μs-ms enzyme motions in the apo- and substrate-mimicked state. J Am Chem Soc. 2005; 127:9167–9176. doi: 10.1021/ja0514949 PMID: 15969595
4. Boehr DD, McElheny D, Dyson HJ, Wright PE. The dynamic energy landscape of dihydrofolate reductase catalysis. Science. 2006; 313:1638–1642. doi: 10.1126/science.1130258 PMID: 16973882
5. Henzler-Wildman KA, Thai V, Lei M, Ott M, Wolf-Watz M, Fenn T, et al. Intrinsic motions along an enzymatic reaction trajectory. Nature. 2007; 450:838–844. doi: 10.1038/nature06410 PMID: 18026086
6. Tang C, Schwieters CD, Clore GM. Open-to-closed transition in apo maltose-binding protein observed by paramagnetic NMR. Nature. 2007; 449:1078–1082. doi: 10.1038/nature06232 PMID: 17960247
7. Lange OF, Lakomek NA, Fares C, Schröder GF, Walter KFA, Becker S, et al. Recognition dynamics up to microseconds revealed from an RDC-derived ubiquitin ensemble in solution. Science. 2008; 320:1471–1475. doi: 10.1126/science.1157092 PMID: 18556554
8. Kim E, Lee S, Jeon A, Choi JM, Lee HS, Hohng S, et al. A single-molecule dissection of ligand binding to a protein with intrinsic dynamics. Nat Chem Biol. 2013; 9:313–318. doi: 10.1038/nchembio.1213 PMID: 23502425
9. Munro JB, Gorman J, Ma X, Zhou Z, Arthos J, Burton DR, et al. Conformational dynamics of single HIV-1 envelope trimers on the surface of native virions. Science. 2014; 346:759–763. doi: 10.1126/science.1254426 PMID: 25298114
10. Ghoneim M, Spies M. Direct correlation of DNA binding and single protein domain motion via dual illumination fluorescence microscopy. Nano Lett. 2014; 14:5920–5931. doi: 10.1021/nl502890g PMID: 25204359
11. Ma B, Kumar S, Tsai CJ, Nussinov R. Folding funnels and binding mechanisms. Protein Eng. 1999; 12:713–720. doi: 10.1093/protein/12.9.713 PMID: 10506280
12. Koshland DE. Application of a theory of enzyme specificity to protein synthesis. Proc Natl Acad Sci USA. 1958; 44:98–104. doi: 10.1073/pnas.44.2.98 PMID: 16590179
13. Weikl TR, Paul F. Conformational selection in protein binding and function. Protein Sci. 2014; 23:1508–1518. doi: 10.1002/pro.2539 PMID: 25155241
14. Bosshard HR. Molecular recognition by induced fit: How fit is the concept? News Physiol Sci. 2001; 16:171–1733. PMID: 11479367
15. Sullivan SM, Holyoak T. Enzymes with lid-gated active sites must operate by an induced fit mechanism instead of conformational selection. Proc Natl Acad Sci USA. 2008; 105:13829–13834. doi: 10.1073/pnas.0805364105 PMID: 18772387
16. Weikl TR, von Deuster C. Selected-fit versus induced-fit protein binding: kinetic differences and mutational analysis. Proteins. 2009; 75:104–110. doi: 10.1002/prot.22223 PMID: 18798570
17. Boehr DD, Nussinov R, Wright PE. The role of dynamic conformational ensembles in biomolecular recognition. Nat Chem Biol. 2009; 5:789–796. doi: 10.1038/nchembio.232 PMID: 19841628
18. Hammes GG, Chang YC, Oas TG. Conformational selection or induced fit: a flux description of reaction mechanism. Proc Natl Acad Sci USA. 2009; 106:13737–13741. doi: 10.1073/pnas.0907195106 PMID: 19666553
19. Wlodarski T, Zagrovic B. Conformational selection and induced fit mechanism underlie specificity in noncovalent interactions with ubiquitin. Proc Natl Acad Sci USA. 2009; 106:19346–19351. doi: 10.1073/pnas.0906966106 PMID: 19887638
20. Changeux JP, Edelstein S. Conformational selection or induced fit? 50 years of debate resolved. F1000 Biol Rep. 2011; 3:19. doi: 10.3410/B3-19 PMID: 21941598
21. Weikl TR, Boehr DD. Conformational selection and induced changes along the catalytic cycle of *Escherichia coli* dihydrofolate reductase. Proteins. 2012; 80:2369–2383. doi: 10.1002/prot.24123 PMID: 22641560
22. Vogt AD, Di Cera E. Conformational selection or induced fit? A critical appraisal of the kinetic mechanism. Biochemistry. 2012; 51:5894–5902. doi: 10.1021/bi3006913 PMID: 22775458
23. Kiefhaber T, Bachmann A, Jensen KS. Dynamics and mechanisms of coupled protein folding and binding reactions. Curr Opion Struct Biol. 2012; 22:21–29. doi: 10.1016/j.sbi.2011.09.010
24. Vogt AD, Pozzi N, Chen Z, Di Cera E. Essential role of conformational selection in ligand binding. Biophys Chem. 2014; 186:13–21. doi: 10.1016/j.bpc.2013.09.003 PMID: 24113284
25. Pozzi N, Vogt AD, Gohara DW, Di Cera E. Conformational selection in trypsin-like proteases. Curr Opin Struct Biol. 2012; 22:421–431. doi: 10.1016/j.sbi.2012.05.006 PMID: 22664096

26. Daniels KG, Tonthat NK, McClure DR, Chang YC, Liu X, Schumacher MA, et al. Ligand concentration regulates the pathways of coupled protein folding and binding. J Am Chem Soc. 2014; 136:822–825. doi: 10.1021/ja4086726 PMID: 24364358

27. Daniels KG, Suo Y, Oas TG. Conformational kinetics reveals affinities of protein conformational states. Proc Natl Acad Sci USA. 2015; 112:9352–9357. doi: 10.1073/pnas.1502084112 PMID: 26162682

28. Chakrabarti KS, Agafonov RV, Pontiggia F, Otten R, Higgins MK, Schertler GFX, et al. Conformational selection in a protein-protein interaction revealed by dynamic pathway analysis. Cell Reports. 2016; 14:32–42. doi: 10.1016/j.celrep.2015.12.010 PMID: 26725117

29. James LC, Roversi P, Tawfik DS. Antibody multispecificity mediated by conformational diversity. Science. 2003; 299:1362–1367. doi: 10.1126/science.1079731 PMID: 12610298

30. Heredia VV, Thomson J, Nettleton D, Sun S. Glucose-induced conformational changes in glucokinase mediate allosteric regulation: transient kinetic analysis. Biochemistry. 2006; 45:7553–7562. doi: 10.1021/bi060253q PMID: 16768451

31. Kim YB, Kalinowski SS, Marcinkeviciene J. A pre-steady state analysis of ligand binding to human glucokinase: Evidence for a preexisting equilibrium. Biochemistry. 2007; 46:1423–1431. doi: 10.1021/bi0617308 PMID: 17260972

32. Tummino PJ, Copeland RA. Residence time of receptor-ligand complexes and its effect on biological function. Biochemistry. 2008; 47:5481–5492. doi: 10.1021/bi8002023 PMID: 18412369

33. Antoine M, Boutin JA, Ferry G. Binding kinetics of glucose and allosteric activators to human glucokinase reveal multiple conformational states. Biochemistry. 2009; 48:5466–5482. doi: 10.1021/bi900374c PMID: 19459610

34. Vogt AD, Di Cera E. Conformational selection is a dominant mechanism of ligand binding. Biochemistry. 2013; 52:5723–5729. doi: 10.1021/bi400929b PMID: 23947609

35. Gianni S, Dogan J, Jemth P. Distinguishing induced fit from conformational selection. Biophys Chem. 2014; 189:33–39. doi: 10.1016/j.bpc.2014.03.003 PMID: 24747333

36. Vogt AD, Chakraborty P, Di Cera E. Kinetic dissection of the pre-existing conformational equilibrium in the trypsin fold. J Biol Chem. 2015; 290:22435–22445. doi: 10.1074/jbc.M115.675538 PMID: 26216877

37. Jarosz AF, Wiley J. What are the odds? A practical guide to computing and reporting Bayes factors. J Problem Solving. 2014; 7:2. doi: 10.7771/1932-6246.1167

38. Peuker S, Cukkemane A, Held M, Noé F, Kaupp UB, Seifert R. Kinetics of ligand-receptor interaction reveals an induced-fit mode of binding in a cyclic nucleotide-activated protein. Biophys J. 2013; 104:63–74. doi: 10.1016/j.bpj.2012.11.3816 PMID: 23332059

39. Greives N, Zhou HX. Both protein dynamics and ligand concentration can shift the binding mechanism between conformational selection and induced fit. Proc Natl Acad Sci USA. 2014; 111:10197–10202. doi: 10.1073/pnas.1407545111 PMID: 24982141

40. Suddala KC, Wang J, Hou Q, Walter NG. Mg^{2+} shifts ligand-mediated folding of a riboswitch from induced-fit to conformational selection. J Am Chem Soc. 2015; 137:14075–14083. doi: 10.1021/jacs.5b09740 PMID: 26471732

41. Mathematica, Version 10.3. Wolfram Research, Inc., Champaign, Illinois; 2015.

42. Storn R, Price K. Differential evolution—a simple and efficient heuristic for global optimization over continuous spaces. J Global Optim. 1997; 11:341–359. doi: 10.1023/A:1008202821328

43. Cavanaugh JE. Unifying the derivations of the Akaike and corrected Akaike information criteria. Stat Probabil Lett. 1997; 31:201–208. doi: 10.1016/S0167-7152(96)00128-9

44. Jaynes ET. Probability theory: the logic of science. Cambridge University Press; 2003.

45. Strachan RW, van Dijk HK. Improper priors with well-defined Bayes factors. Liverpool, L69 7ZA, United Kingdom: Department of Economics and Accounting, University of Liverpool; 2005. EI 2004–18.